Journal of Receptors and Signal Transduction

ISSN: 1079-9893 (Print) 1532-4281 (Online) Journal homepage: https://www.tandfonline.com/loi/irst20

Cytotoxic oxindole derivatives: *in vitro* EGFR inhibition, pharmacophore modeling, 3D-QSAR and molecular dynamics studies

Sasikala Maadwar & Rajitha Galla

To cite this article: Sasikala Maadwar & Rajitha Galla (2019): Cytotoxic oxindole derivatives: *in vitro* EGFR inhibition, pharmacophore modeling, 3D-QSAR and molecular dynamics studies, Journal of Receptors and Signal Transduction, DOI: 10.1080/10799893.2019.1683865

To link to this article: https://doi.org/10.1080/10799893.2019.1683865

Published online: 09 Dec 2019.

JOURNAL OF RECEPTORS AND SIGNAL TRANSDUCTION
https://doi.org/10.1080/10799893.2019.1683865

Taylor & Francis
Taylor & Francis Group

RESEARCH ARTICLE

Cytotoxic oxindole derivatives: *in vitro* EGFR inhibition, pharmacophore modeling, 3D-QSAR and molecular dynamics studies

Sasikala Maadwar[a,b] and Rajitha Galla[a]

[a]Institute of Pharmaceutical Technology, Sri Padmavati Mahila Visvavidyalayam, Tirupati, India; [b]Medicinal Chemistry and Pharmacology Division, Indian Institute of Chemical Technology, Hyderabad, India

ABSTRACT

Epidermal growth factor receptor (EGFR) is one of the vital protein targets in many solid tumors and is an attractive target for developing new drugs. In this study we have focused on elucidation of the mechanistic insights of cytotoxic potentials of oxindole derivatives using various *in vitro* and molecular modeling techniques. *In vitro* EGFR inhibition assay is performed with the potent cytotoxic oxindole compounds which are previously proved for their cytotoxic activity against breast cancer (MCF7) and ovarian cancer (SKVO3) cell lines. Molecular docking studies against kinase domain of EGFR protein revealed the probable interactions of oxindole derivatives. Pharmacophore modeling studies had identified a pharmacophore model with three hydrogen bond acceptors and three aromatic rings (AAARRR.1003) as a potential model for cytotoxic activity against MCF7 cell lines and validated through 3D QSAR studies resulting in superior regression scores ($r^2 = 0.92$, $q^2 = 0.80$ and Pearson $R = 0.95$). Molecular dynamic studies have revealed the conformational changes in the EGFR-compound 2complex during the 25 ns simulation time frame.

ARTICLE HISTORY
Received 5 September 2019
Accepted 7 October 2019

KEYWORDS
Oxindoles; EGFR; docking; pharmacophore modeling; 3D QSAR; molecular dynamics

Introduction

Cancer is considered as a major cause for increased death rate in humans. Among women, breast cancer is the most prevalent and ovarian cancer is genital system related cancers with an estimate of 255,180 and 22,440 new cases, respectively [1]. Stanley Cohen, Nobel Prize Laureate in Physiology/Medicine, discovered epidermal growth factor (EGFR) 25 years ago and elucidated its role in cell growth. This furthered knowledge on signaling events in cancer biology and enabled to face challenges posed by the abnormal cellular events resulting in cancer. Epidermal growth factor receptors (EGFRs) are a large family of receptor tyrosine kinases (TK) expressed in several types of cancer, including breast, lung, esophageal, and head and neck. EGFR and its family members are the major contributors of a complex signaling cascade that modulates growth, signaling, differentiation, adhesion, migration and survival of cancer cells. [2].

Isatin is an oxindole containing heterocyclic moiety, an endogenous compound isolated in 1988 and reported to possess a wide range of biological activities including anticancer [3], antidepressant [4], anticonvulsant [5], antifungal [6], anti-HIV [7], anti-inflammatory [8]. During past decades, researchers have embarked on the development of new isatin based anticancer agents [9–11]. Owing to these properties, derivatives of isatin have been developed for therapeutic applications. Recently, a 5-fluoro-3-substituted-2-oxoindole derivative compound SU11248 [Sutent] received FDA approval for the treatment of gastrointestinal stromal tumors and advanced renal cell carcinoma [12]. Substituted isatins have been proved for their EGFR inhibitory activity [13].

In the present work, in order to elucidate the mechanistic insights of the disubstituted oxindole molecules we have evaluated them for their *in vitro* EGFR inhibition which we have previously proved their cytotoxic potentials against human breast and ovarian cancer cell lines. Synthesis of these compounds is shown in the Scheme 1 [14–15]. Further we have performed docking studies against EGFR protein. Additionally, pharmacophore modeling studies were performed for dataset of oxindole derivatives to identify the potential model for cytotoxic activity against MCF7 cell lines and validated through 3D QSAR studies. Additionally, molecular dynamics simulations are conducted to elucidate the conformational changes of the EGFR-oxindole complex.

Materials and methods

In vitro *EGFR inhibition*

The compounds with higher cytotoxic activity were selected for evaluation of EGFR inhibition using Kinase-Glo Plus luminescence kinase assay kit and IC_{50} values were calculated by measuring the protein kinase generated ADP [16]. Test compounds selected for the assay were diluted to 100 mM in 10% DMSO from which, 5 mL was added to a 50 mL reaction mixture (10 mM $MgCl_2$, 40 mM Tris, pH 7.4, 0.1 mg/mL BSA, 0.2 mg/mL Poly [Glu, Tyr] substrate, 10 mM ATP and EGFR) and reactions were conducted at 30 °C for 40 min. Following, 50 mL of assay

CONTACT Sasikala Maadwar maadwarsasikala@gmail.com Institute of Pharmaceutical Technology, Sri Padmavati Mahila Visvavidyalayam, Tirupati, India.

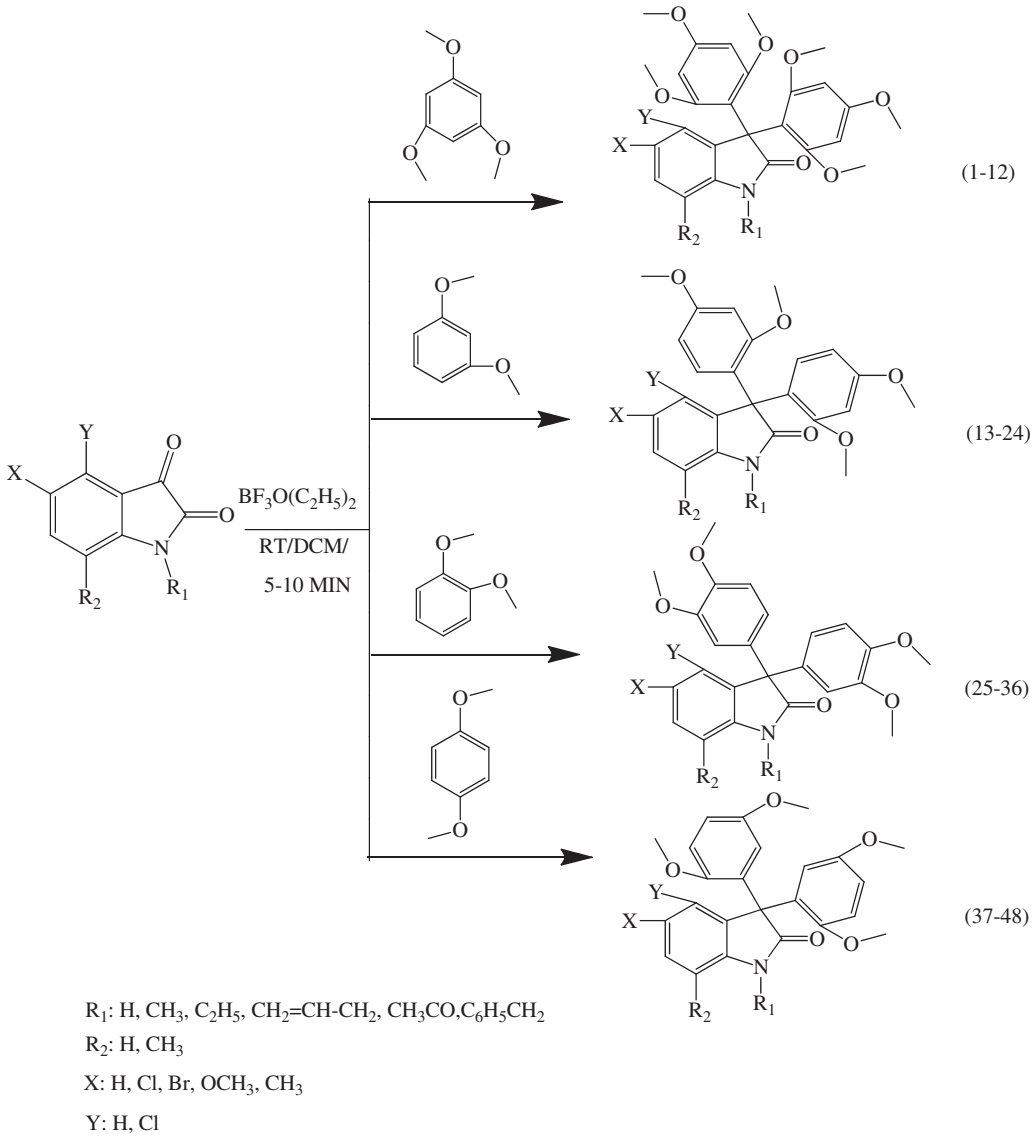

Scheme 1. Synthesis of data set compounds.

solution was added to each reaction and incubated at room temperature for 5 min. The reaction mixture was incubated in a 96-well plate at 30 °C for 30 min and the reaction was terminated by adding 25 mL of ADP-Glo reagent. The 96-well plate was shaken and then incubated for 30 min at ambient temperature. ADP was generated from the protein kinase reaction by adding 50 mL of kinase detection reagent and resulted in an increase in luminescence signal in the presence of ADP-Glo assay kit. Blank control was set up and the corrected activity for each protein kinase target was determined by removing the blank control value. Additionally, regression analysis was performed to determine the correlation between MCF7 cytotoxicity and EGFR inhibition of the tested compounds.

Molecular modelling and 3D QSAR studies

Dataset ligands

Substitutions of 48 newly synthesized di- and tri- methoxy oxindole derivatives were shown in Table 1. 2D structures were geometrically optimized to 3D and energy was minimized by using the Ligprep tool of Schrodinger suite and applying Optimized Potentials for Liquid Simulations (OPLS - 2005) Force Field. Molecular properties and ADME profiling was performed using Qikprop module of Schrodinger Suite to selected compounds which were geometrically optimized.

Molecular docking studies

Initially, digital structure of the target kinase domain of EGFR was retrieved from the Protein data bank website with PDB Id: 1M17. Protein structure was optimized using Protein preparation wizard. Protein structure was corrected by deleting all non-interacted water molecules and added hydrogen atoms to satisfy the valences and optimized by using OPLS-2005 force field. Glide XP docking protocol was used for molecular docking studies [17]. Glide XP modules include two basic steps, Receptor Grid generation and ligand docking. A grid was generated considering the volume of the active binding pocket of the protein and all ligands were docked into the active site of the target protein. Glide score

Table 1. Experimental and predicted cytotoxicity against MCF7/Wt cell lines.

						Atom-based QSAR		
Compound no.	R_1	R_2	X	Y	pIC_{50} experimental	Pharm set	pIC_{50} predicted	Data set
	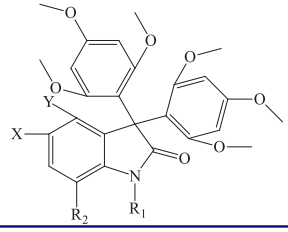							
1	H	H	H	H	4.731	Inactive	4.72	Training
2	H	H	Cl	H	5.143	Active	5.11	Training
3	H	H	Br	H	5.114	Active	5.12	Training
4	CH3	H	H	H	4.87	Active	4.80	Training
5	H	H	OCH3	H	4.74	Inactive	4.78	Training
6	C6H5–CH2	H	H	H	4.545	Inactive	4.72	Test
7	H	CH3	CH3	H	4.635	Inactive	4.67	Training
8	H	H	H	Cl	4.618	Inactive	4.57	Training
11	CH2–CH–CH2	H	H	H	4.833	Active	4.86	Training
12	H	H	CH3	H	4.735	Inactive	4.73	Training
	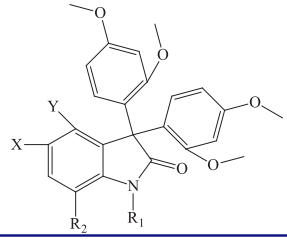							
13	H	H	H	H	4.73	Inactive	4.70	Test
14	H	H	Cl	H	4.53	Inactive	4.57	Training
15	H	H	Br	H	4.67	Inactive	4.67	Training
16	CH3	H	H	H	4.458	Inactive	4.42	Training
17	H	H	OCH3	H	4.389	Inactive	4.42	Test
18	C6H5–CH2	H	H	H	5.036	Active	5.04	Training
19	H	CH3	CH3	H	4.728	Inactive	4.74	Training
20	H	H	H	Cl	5.097	Active	5.09	Training
21	C2H5	H	H	H	4.813	Active	4.83	Training
22	CH3–CO	H	H	H	4.86	Active	4.85	Training
23	CH2–CH–CH2	H	H	H	4.914	Active	4.93	Training
24	H	H	CH3	H	4.907	Active	4.90	Training
	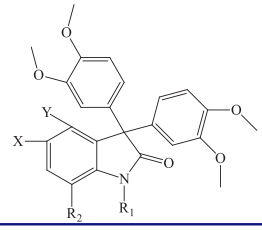							
25	H	H	H	H	4.807	Active	4.74	Test
26	H	H	Cl	H	4.955	Active	4.87	Test
27	H	H	Br	H	4.955	Active	4.93	Training
28	CH3	H	H	H	4.767	Active	4.81	Training
29	H	H	OCH3	H	4.742	Inactive	4.66	Test
30	C6H5–CH2	H	H	H	4.747	Inactive	4.77	Training
31	H	CH3	CH3	H	4.775	Active	4.80	Training
32	H	H	H	Cl	4.917	Active	4.91	Training
33	C2H5	H	H	H	4.857	Active	4.86	Training
34	CH3–CO	H	H	H	4.967	Active	4.99	Training
35	CH2–CH–CH2	H	H	H	4.925	Active	4.89	Test
36	H	H	CH3	H	4.943	Active	4.89	Training

(*continued*)

Table 1. Continued.

Compound no.	R_1	R_2	X	Y	pIC_{50} experimental	Atom-based QSAR		
						Pharm set	pIC_{50} predicted	Data set
	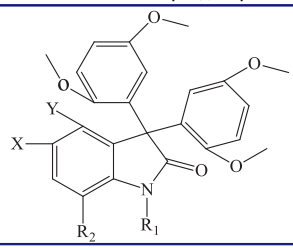							
37	H	H	H	H	4.839	Active	4.83	Training
38	H	H	Cl	H	4.914	Active	4.79	Test
39	H	H	Br	H	4.791	Active	4.80	Training
40	CH3	H	H	H	4.821	Active	4.82	Test
41	H	H	OCH3	H	4.815	Active	4.84	Training
42	C6H5–CH2	H	H	H	4.833	Active	4.86	Training
43	H	CH3	CH3	H	5.036	Active	5.04	Training
44	H	H	H	Cl	4.955	Active	4.98	Training
45	C2H5	H	H	H	4.914	Active	4.84	Training
46	CH3–CO	H	H	H	4.839	Active	4.81	Training
47	CH2–CH–CH2	H	H	H	4.742	Inactive	4.79	Training
48	H	H	CH3	H	4.943	Active	4.92	Training

includes a steric-clash term, adds polar terms featured by Schrodinger to correct electrostatic mismatches. Glide score is a combination of hydrophilic, hydrophobic, metal binding groups, Van der Waals energy, freezing rotatable bonds and polar interactions with receptor.

Pharmacophore modelling and 3D-QSAR studies

By the allocation of activity threshold range whole data set was fractioned into active ($pIC_{50}>4.75$) and inactive ($pIC_{50}<4.75$). These ligands were internally validated through PHASE module to generate/identify series of common pharmacophore hypotheses [18,19]. A 3D pharmacophore model was developed using a set of pharmacophore features to generate sites for all the compounds, concurring with various chemical features that may make easy non-covalent binding among the ligand and its binding pocket. Distinctive six pharmacophore features are hydrogen bond acceptor (A), hydrogen bond donor (D), hydrophobic group (H), negatively ionizable (N), positively ionizable (P) and aromatic ring (R). Maximum of six and a minimum of five sites were selected in order to obtain an efficient pharmacophore model. Hypotheses were generated by a systematic variation of number of sites (n_{sites}) and the number of matching active compounds (n_{act}). With $n_{act} = n_{act\ -\ tot}$. Initially ($n_{act\ -\ tot}$) is the total number of active compounds in the training set, n_{sites}. The scoring protocol provides a ranking of different hypotheses to choose the most appropriate for further investigation.

Pharmacophore-based QSAR studies were performed by choosing best common pharmacophore hypothesis. 80% of dataset ligands were randomly selected as training set and remaining as test set. Different QSAR models were generated, each containing upto 7 PLS factors through regression analysis. Leave one-out (LOO) and leave-half-out (LHO) cross-validation provided the predictive value of the models. The cross validated coefficient, r^2_{cv}, was calculated using the following equation:

$$r^2_{cv} = 1 - \frac{\sum (Y_{predicted} - Y_{observed})^2}{\sum (Y_{observed} - Y_{mean})^2} \quad (1)$$

where $Y_{predicted}$, $Y_{observed}$ and Y_{mean} are the predicted, observed and the mean values of the target property (pIC50), respectively. $(Y_{observed} - Y_{mean})^2$ is the predictive residual sum of squares (PRESS). The predictive correlation coefficient (r^2_{pred}), based on molecules of the test set, is defined as follows:

$$r^2_{pred} = \frac{SD - PRESS}{SD} \quad (2)$$

where SD is the sum of the squared deviation between the biological activities of the test set and mean activities of the training set molecules, PRESS is the sum of squared deviation between predicted and actual activity values for every molecule in the test set. According to the literature, 3D-QSAR models were accepted if

$$r^2 > 0.6;\ r^2_{cv}(q^2) > 0.5 \quad (3)$$

Molecular dynamics

The docked complexes of EGFR protein and compound 2 was selected for molecular dynamics studies using Desmond by D.E. Shaw Research [20,21] as discussed by Gade et al., 2018). Molecular dynamic simulations were performed for 25 ns for each complex using TIP4PEW water solvent model, and neutralized by adding sodium ions. The system was maintained at 0.15 M salt concentration (Na^+ Cl^-) simulating the physiological condition and dynamics simulation were performed using OPLS 2005 force field and NPT

ensemble(constant number of atoms, at constant pressure [1.01352 bar], and constant temperature [300K] for 25 ns. For system ensemble, Nose–Hoover chain thermostat with a relaxation time of 1 ps and Martyna–Tobias–Klein barostat with 2 ps relaxation time and isocratic cooling style and Coulombic interactions were cut off at 9 A^{o} radius were used.

Results and discussions

In vitro *EGFR inhibition*

Out of 48 compounds which are previously synthesized in our laboratory, a total of 15 compounds with relatively higher cytotoxic activity against MCF7 cell lines were chosen for *in vitro* EGFR inhibition assay. Inhibitory concentrations (μM) were ranged between 3.09 ± 1.48 (compound 2) and 30.20 ± 2.18 (compound 23) (Table 2). The chloro-substitution at fifth position on oxindole nucleus of compound 2, resulting in the resonance effect, could be the reason for the relatively higher EGFR inhibitory activity. Among the compounds with halo-substitution, chloro substituted compounds were more active when compared to bromo substituted compounds, whereas, among the compounds with alkyl substitutions methyl and allyl substituted derivatives were more active when compared to ethyl substituted compound. Overall, oxindole derivatives with halo (chloro and bromo substitution at fourth and fifth position) and alkyl (methyl at fifth position and allyl at first position) were reported with relatively higher activity.

Molecular docking studies

Molecular docking studies were performed to determine the protein-ligand interactions and also to understand the conformational changes in the protein-ligand complex. Docking studies were performed with the compounds which were evaluated for *in vitro* EGFR inhibition. Docking scores of these compounds were ranged between −2.086 (compound 18) and −5.206 (compound 45). Most commonly interacted protein residues through hydrogen bonds include ARG 817

Table 2. *In vitro* and *in silico* EGFR inhibition studies of Novel Istain derivatives.

Compound	EGFR inhibition in terms of IC_{50} value (μM)	Dock score	No. of H-bonds	Interacting amino acids	H bond distance (Å)	Binding energy
2	3.09 ± 1.48	−2.86	2	LYS 851	2.01	−41.224458
				GLY 833	2.40	
3	4.11 ± 0.86	−2.186	2	ARG 817	2.14	−34.509403
				CYS 773	2.04	
20	5.28 ± 1.47	−2.988	2	ARG 817	2.05	−41.271329
				ASN 818	2.63	
43	5.63 ± 0.92	−3.757	1	ARG 817	2.45	−27.1737818
18	8.92 ± 2.18	−2.086	2	ARG 817	2.17	−36.063729
				LYS 721	2.05	
34	9.27 ± 1.29	−3.822	3	CYS 773	2.09	−51.462836
				LYS 721	2.30, 2.08	
26	11.71 ± 1.83	−3.62	1	ARG 817	1.95	−48.169181
27	12.85 ± 1.68	−5.088	0	–	–	−57.645734
44	13.26 ± 1.39	−3.305	2	ARG 817	1.80	−43.294269
				CYS 773	2.04	
48	14.09 ± 0.97	−2.967	1	ARG 817	1.97	−32.542379
35	23.61 ± 2.28	−5.079	0	–	–	−60.1305874
36	24.50 ± 1.00	−5.095	1	LEU 694	1.72	−54.604515
32	27.53 ± 2.47	−3.971	1	LYS 721	1.98	−40.899004
45	28.57 ± 2.81	−5.206	0	–	–	−56.013714
23	30.20 ± 2.18	−4.605	0	–	–	−59.013236
Gefitinib	0.062 ± 0.009	–	–	–	–	–

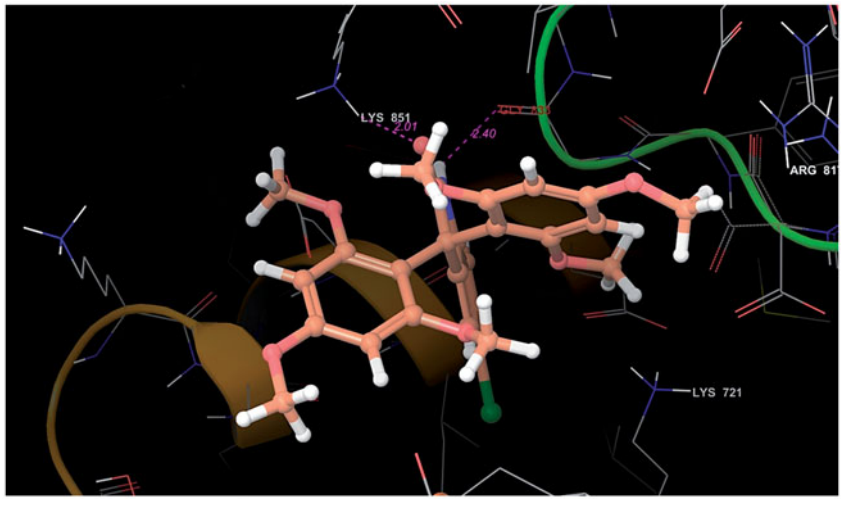

Figure 1. Ligand binding mode of compound 2 with kinase domain of EGFR protein.

and CYS 773. Hydrogen bonding was also identified between protein residues such as LYS 721, ASN 818, GLY 833, LYS 851, LEU 694 and CYS 773. However, for compounds such as 23, 27, 35 and 45 no contribution of H-bonding in the binding interaction was observed. Binding interaction profile of the most active EGFR inhibitor (compound 2) among the series was shown in Figure 1. Protein-ligand binding energies of the docked compounds were determined through post docking calculations and revealed that compound 35 was having highest binding energy (–60.13 kcal) among the series. Dock scores, binding profile and binding energies for the evaluated compounds were shown in Table 2.

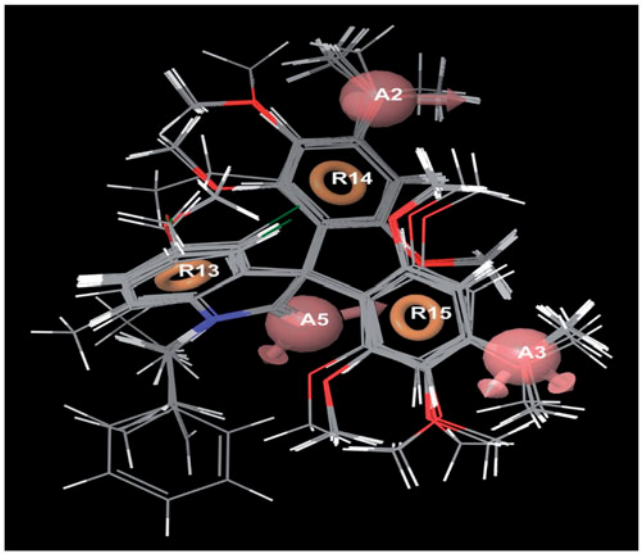

Figure 2. 3D spatial arrangement of the common pharmacophore AAARRR.1003.

Table 3. Regression scores of AAARRR.1003.

Hypothesis	Factors	F	R^2	Q^2	Pearson R
AAARRR.1003	1	15.9	0.313	0.2458	0.6732
	2	17.4	0.5056	0.5863	0.8607
	3	24.1	0.6867	0.5718	0.8059
	4	33.4	0.8067	0.7107	0.8752
	5	37.8	0.8591	0.7109	0.8875
	6	51.5	0.9115	0.7989	0.9494
	7	91.8	0.9568	0.7617	0.8948

Pharmacophore modelling and 3D QSAR studies

A total of 70 hypotheses with 6 pharmacophore features were obtained. Of the 70 common pharmacophore hypotheses, a six feature pharmacophoric model, AAARRR.1003 constituting three hydrogen bond acceptors and three aromatic ring systems was identified as most suitable pharmacophore model. The 3D spatial arrangement of the 6 pharmacophoric features of AAARRR.1003 and overlapping of data set ligands over the obtained pharmacophore model were shown in Figure 2. A potential QSAR model for the dataset ligands over AAARRRR.1003 hypothesis was built by employing partial least squares (PLS) regression analysis and the results were tabulated in Table 3. Regression analysis of total 7 factors were given of which result of PLS-7 was considered to be the best as the regression coefficients r^2 is 0.96 (for training set), q^2 is 0.76 (for test set) and Pearson-R is 0.90. Predicted activity of all the dataset ligands obtained from QSAR studies considering PLS 7 were listed in Table 1. The plots of experimental activity versus predicted activity of all

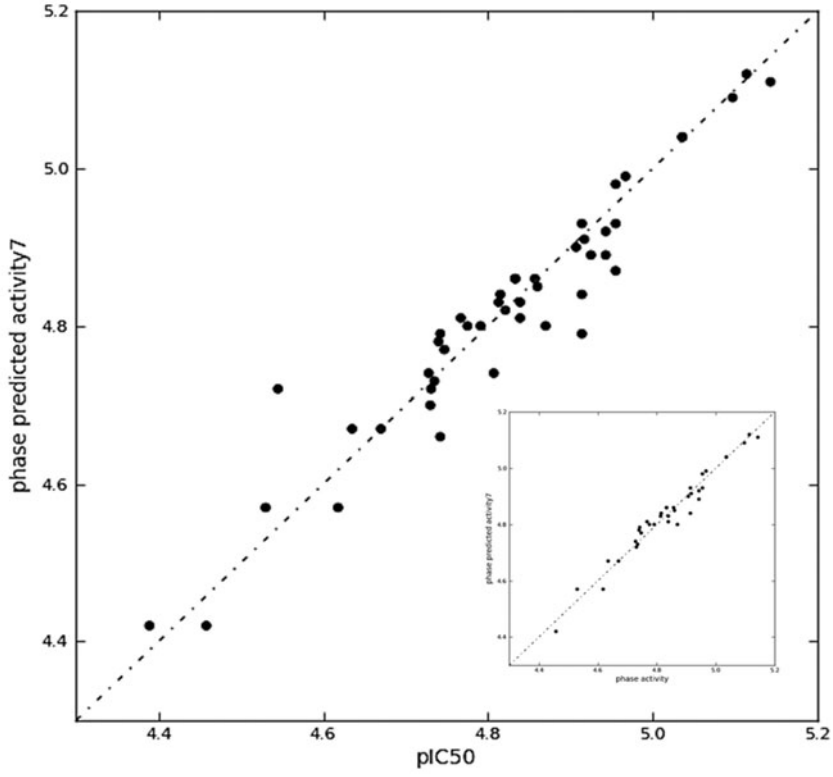

Figure 3. Fitness of predicted vs actual pIC_{50} for all data set ligands and training set ligands (inset).

dataset ligands and training set ligands were shown in Figure 3.

Molecular dynamics

Molecular dynamics simulations performed in the solvent environment at constant temperature and pressure has revealed the confirmation changes of the EGFR-compound 2 complex. Stability of the complex is determined in terms of the RMSD and RMSF of the protein components along with the ligand. Root mean square fluctuation (RMSF) is useful for characterizing local changes along the protein chain. During the simulation, fluctuations in the N- and C-terminals of the protein were more than any other part of the protein. Particularly, the Cα and side chain residues in the loop region of the C-terminal has reported greater fluctuations (RMSF) beyond 22.5 A^0. Majority of the interactions were observed in the beta-strands of the protein (Figure 4). Root Mean Square Deviation (RMSD) is used to measure the average change in displacement of a selection of atoms for a particular frame with respect to a reference frame. EGFR-compound 2 complex was in stable confirmation until 15 ns. However, there is a sudden spike in the RMSD values of Cα and side chain amino acids immediately 15 ns and larger deviation was observed at 20 ns, later in the last few ns of the simulation, complex seems to be stable at higher RMSD value. Similar to the deviations observed in the protein structure, larger deviations were recorded from 15 ns (Figure 5).

Over the simulation period, total number of protein-ligand contacts ranged between one and more than nine contacts. During the simulation time frame ARG 817 was the most interacted amino acid, followed by LEU 820 and MET 769. Interactions with amino acids such as ALA 698, ALA 719, GLU 738, MET 742, LEU 764, PRO 770, PHE 771, CYC 773, ASP 776, ASN 818 and VAL 821 had negligible impact on the overall interaction profile (Figure 6). In this simulation model, hydro-

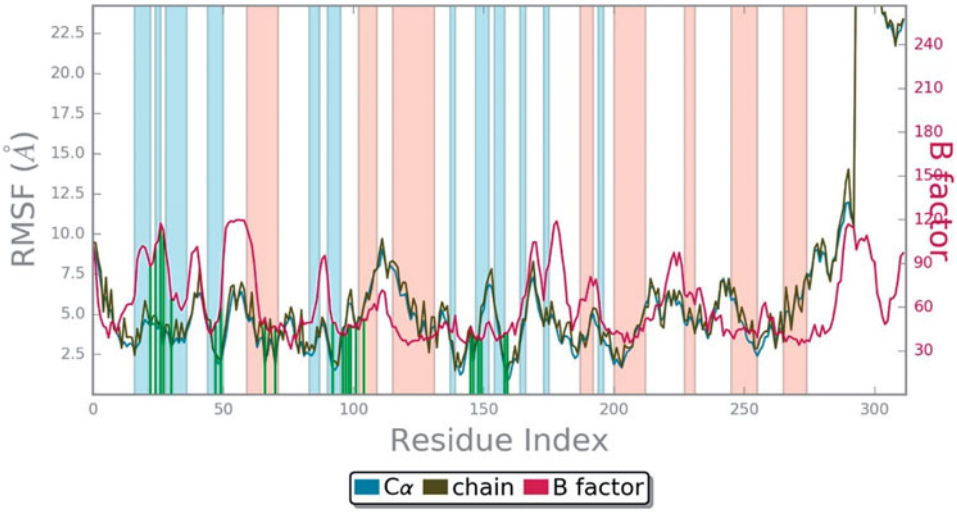

Figure 4. Root mean square fluctuations (RMSF) for the C-alphas and side chain residues of EGFRprotein.

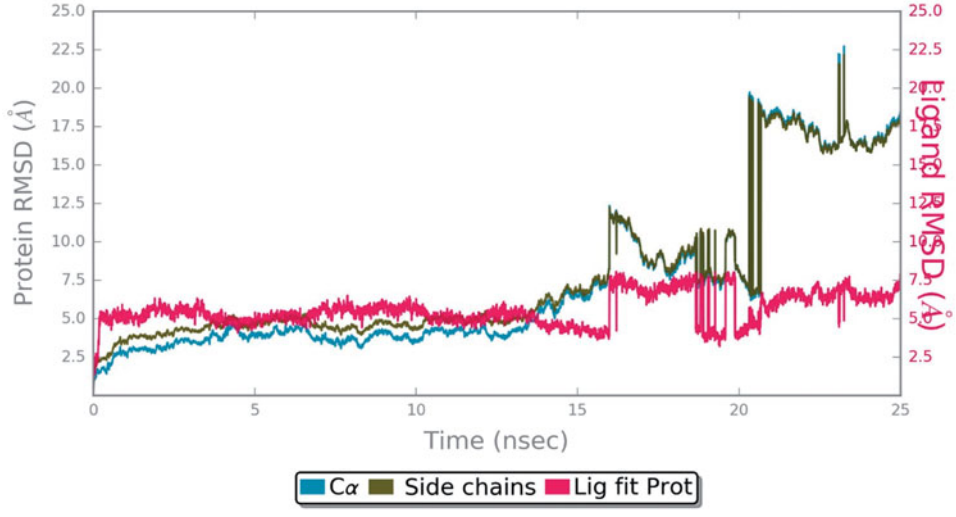

Figure 5. Root mean square deviation (RMSD) of simulated EGFR-compound 2 complex.

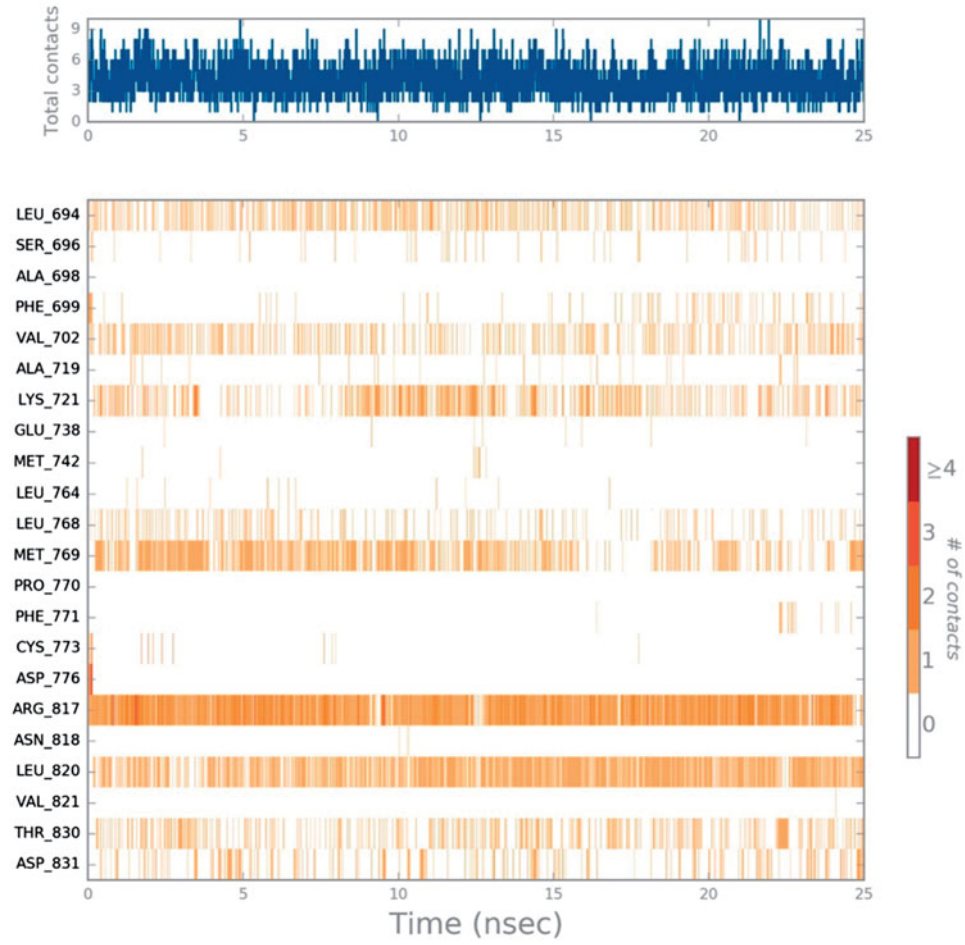

Figure 6. Protein–ligand interaction diagram of protein residues during molecular dynamics simulation.

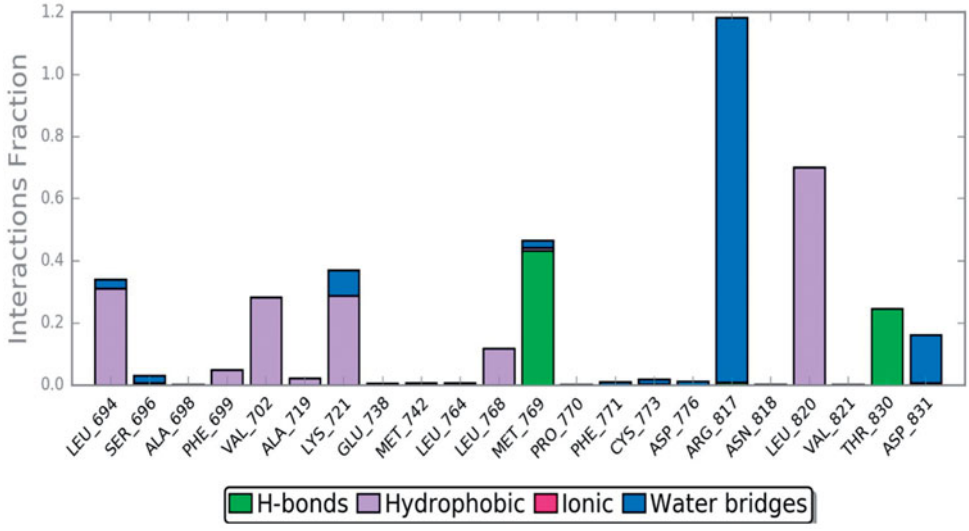

Figure 7. Interaction fractions of various EGFR residues during molecular dynamic simulations.

gen bonds were recorded with MET 769 and THR 830, however, the impact is only transient. Hydrophobic interactions were prominent with LEU 694, LYS 721, VAL 702 and LEU 820 amino acids. Water bridges were recorded with ARG 871 (most prominent) and minor impact with LYS 721 and ASP 831 (Figure 7).

During the 25 ns simulation, deviation in the molecular properties such as ligand RMSD, radius of gyration [rGyr],

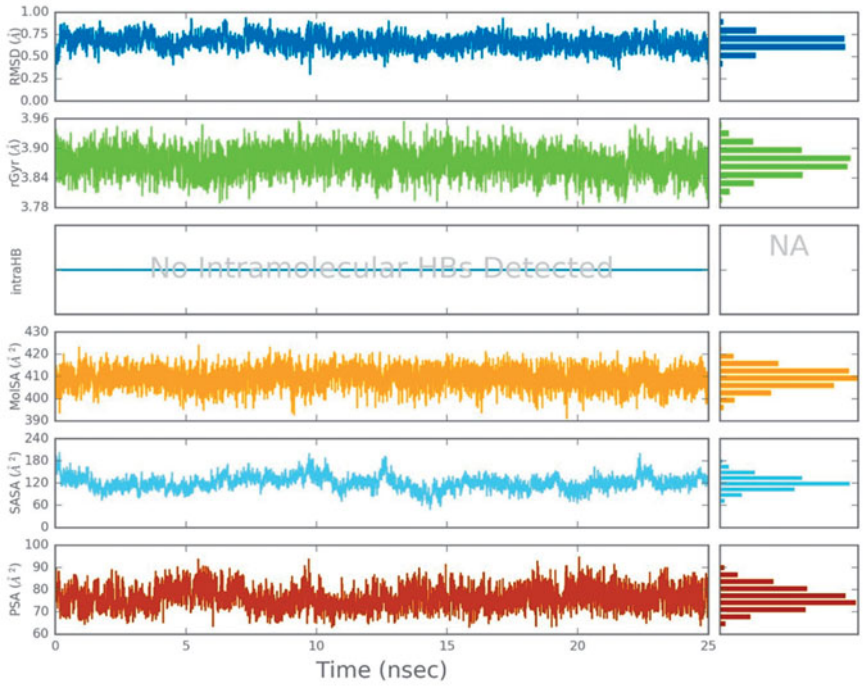

Figure 8. Fluctuations in the compound 2 properties during 25 ns simulation.

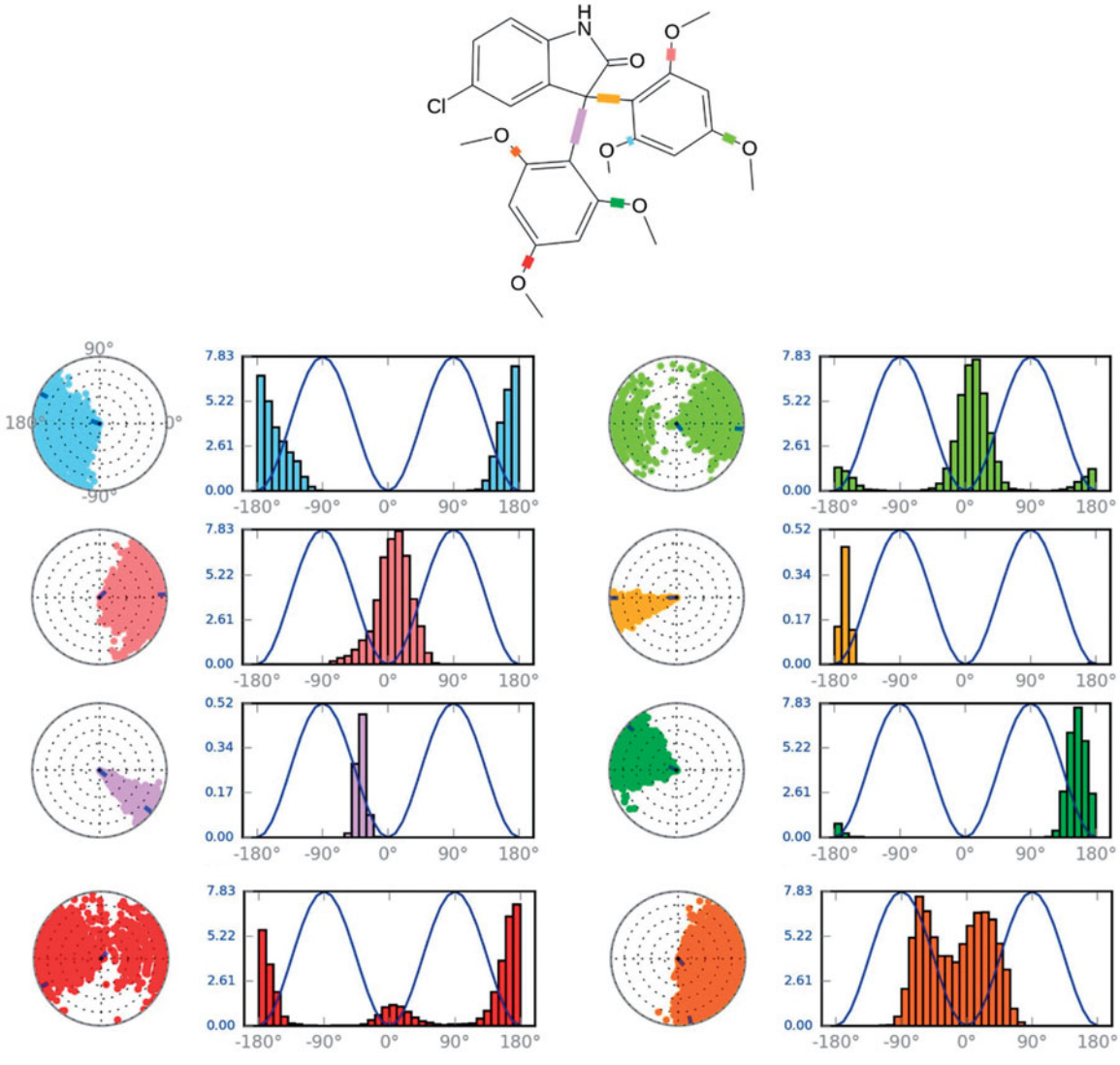

Figure 9. Extent of torsion at each rotational bond.

molecular surface area [MolSA], solvent accessible surface area [SASA], and polar surface area [PSA] of compound 2 was minimal with no intramolecular hydrogen bonds (Figure 8). However, ligand torsion was higher and radially outward with the terminal methoxy groups of both the trimethoxy benzenes attached to the core nucleus (Figure 9).

Conclusion

In the current investigation, a series of novel oxindole derivatives were taken which are previously proved for their cytotoxic potentials. Enzyme inhibitory studies suggested that the inhibitory activity of these compounds against EGFR protein could be the reason for the higher cytotoxicity. Molecular docking studies further supported the elucidation of binding patterns of the molecules in EGFR protein environment. Pharmacophore modeling studies identified AAARRR.1003 common pharmacophore model as a valid model, which was also supported by the employed regression analysis. Results from molecular dynamics simulations elucidated the mechanistic insight of EGFR inhibition by oxindole compounds and their binding phenomenon. Further simulations with longer time period may provide deeper insights of ligand interactions in the protein environment. It is noteworthy to use compound 2 as a new scaffold for further development of multifunctional compounds.

Acknowledgements

The authors thank Dr Sunil Misra (senior scientist, Biology Division, CSIR-IICT, Hyderabad) for providing biological laboratory facilities to perform biological evaluation. The authors also thank Mrs Swetha and Mr Devender (Discovery Labs, CSIR-IICT, Hyderabad), for providing facilities to perform chemical reactions. We would like to acknowledge Mr Reddy G (ddlabs.in, Hyderabad), for writing assistance and editorial support.

Disclosure statement

No potential conflict of interest was reported by the authors.

References

[1] Siegal RL, Millerk D, Jemal A. Cancer statistics. CA Cancer J Clin. 2017;67:7–30.
[2] Parthasarathy S, Moorthy PP, Dhanya H, et al. Targetting the EGFR signalling pathway in cancer therapy. PMC-NCBI. 2012;16(1): 15–31.
[3] Ibrahim HS, Abou-Seri SM, Tanc M, et al. Isatin-pyrazole benzenesulfonamide hybrids potently inhibit tumor-associated carbonic anhydrase isoforms IX and XII. Eur J Med Chem. 2015;103: 583–593.
[4] Rohini R, Reddy PM, Shanker K, et al. Synthesis of mono, bis-2-(2-arylideneaminophenyl) indole azomethines as potential antimicrobial agents. Arch Pharm Res. 2011;34(7):1077–1084.
[5] Verma M, Pandeya SN, Singh KN, et al. Anticonvulsant activity of Schiff bases of isatin derivatives. Acta pharm. 2004;54(1):49–56.
[6] Pandeya SN, Yogeeshwari P. Sri Ram Nath DG. Synthesis, antibacterial and antifungal activities of N-mannich bases of 3-[N2-pyrimethaminylimino] isatin. Indian J Pharm Sci. 2002;64:209–212.
[7] Selvam P, Murugesh N, Chandra Mohan M, et al. Synthesis and antiHIV activity of Novel Isatin-Sulphonamides. Indian J Pharm Sci. 2008;70(6):779–782.
[8] Sridhar SK, Ramesh A. Synthesis and pharmacological activities of hydrazones, Schiff and Mannich bases of isatin derivatives. Biol Pharm Bull. 2001;24(10):1149–1152.
[9] Eldehna WM, Altoukhy A, Mahrous H, et al. Design, synthesis and QSAR study of certain isatin-pyridine hybrids as potential antiproliferative agents. Eur J Med Chem. 2015;90:684–694.
[10] Sharma P, Senwar KR, Jeengar MK, Reddy TS, et al. H_2O-mediated isatin spiroepoxide ring opening with NaCN: Synthesis of novel 3-tetrazolylmethyl-3-hydroxy-oxindole hybrids and their anticancer evaluation. Eur J Med Chem. 2015;104:11–24.
[11] Pervez H, Ramzan M, Yaqub M, et al. Cytotoxic and Phytotoxic Effects of Some New N4-Aryl Substituted Isatin-3-thiosemicarbazones. Med Chem. 2012;8(3):505–514.,
[12] Hamdy AM, Al-Masoudi NA, Pannecouque C, et al. Regioselective synthesis Suziki-Miyaura reaction of 4,7-dichloro-N-methylisatin. Synthesis, anti-HIV activity and modelling studies. RSC Adv. 2015; 5(130):107360–107369.
[13] Yousry AA, Ahmed MS, Amany B, Samir YA, et al. Design synthesis and anti proliferative activity, molecular docking and cell cycle analysis of some novel (morholinosulphonyl)isatins with potential EGFR inhibitory activity. Eur J Med Chem. 2018;156:918–932.
[14] Sasikala M, Rajitha G, Santhosh KG. A facile and efficient synthesis of 3,3 disubstitued oxindole derivatives and their cytotoxic properties. Res J Pharm Technol. 2019;12(3):1091–1095.
[15] Sasikala M, Rajitha G, Santhosh KG. A facile and efficient synthesis of 3,3 disubstitued oxindole derivatives and their cytotoxic properties. Int Res J Pharm. 2019;10(4):190–195.
[16] Babu YR, Bhagavanraju M, Reddy GD, et al. Design and synthesis of quinazolinone tagged acridones as cytotoxic agents and their effects on EGFR tyrosine kinase. Arch Pharm Chem Life Sci. 2014; 347(9):624–634.
[17] Deepak Reddy G, Pavan K, Divya R, et al. Structural insight of JAK 2 inhibitors: pharmacophore modeling and ligand based 3D-QSAR studies of pyrido-indole derivatives. J Recept Signal Transduct. 2014;35(2):189–201.
[18] Rajendra Prasad VVS, Deepak Reddy G, Appaji D, et al. Chemosensitizing acrodones: in vitro calmouldine dependent cAMP phosphodiesterase inhibition, docking, pharmacophore modelling and 3D QSAR studies. J Mol Graph Model. 2013;40: 116–124.
[19] Guttikonda V, Raavi D, Maadwar SK, et al. Molecular insights of benzodipyrazole as CDK2 inhibitors combined molecular docking, molecular dynamics, and 3D QSAR studies. J. Recept Signal Transduct. 2015;35(5):439–449.
[20] Jyothi Buggana S, Paturi MC, Perka H, et al. Novel 2,4-disubstituted quinazolines as cytotoxic agents and JAK2 inhibitors: synthesis, in vitro evaluation and molecular dynamics studies. Comput Biol Chem. 2019;79:110–118.
[21] Gade DR, Makkapati A, Yarlagadda RB, et al. Elucidation of chemosensitization effect of acridones in cancer cell lines: combined pharmacophore modelling, 3D QSAR, and molecular dynamics studies. Comput Biol Chem. 2018;74:63–75.